Towards reversible control of domain wall conduction in Pb(Zr0.2Ti0.8)O3 thin films

I. Gaponenko, P. Tückmantel, J. Karthik, L. W. Martin, and P. Paruch

Citation: Applied Physics Letters **106**, 162902 (2015); doi: 10.1063/1.4918762
View online: http://dx.doi.org/10.1063/1.4918762
View Table of Contents: http://scitation.aip.org/content/aip/journal/apl/106/16?ver=pdfcov
Published by the AIP Publishing

Towards reversible control of domain wall conduction in $Pb(Zr_{0.2}Ti_{0.8})O_3$ thin films

I. Gaponenko,[1,a)] P. Tückmantel,[1] J. Karthik,[2] L. W. Martin,[3,4] and P. Paruch[1]
[1]*Department of Quantum Matter Physics, University of Geneva, 24 Quai Ernest Ansermet, 1211 Geneva 4, Switzerland*
[2]*Department of Materials Science and Engineering and Materials Research Laboratory, University of Illinois, Urbana-Champaign, Urbana, Illinois 61801, USA*
[3]*Department of Materials Science and Engineering, University of California, Berkeley, Berkeley, California 94720, USA*
[4]*Materials Science Division, Lawrence Berkeley National Laboratory, Berkeley, California 94720, USA*

(Received 18 December 2014; accepted 10 April 2015; published online 20 April 2015)

Control over the localised conductance recently observed at ferroelectric domain walls is key for their integration into potential nanoelectronics devices. Using a combination of piezoresponse force microscopy and local conductance mapping, we demonstrate switching between conducting and insulating behavior at 180° domain walls in epitaxial $Pb(Zr_{0.2}Ti_{0.8})O_3$ thin films subjected to ultrahigh vacuum thermal annealing or exposed to ambient conditions, respectively. The reversibility of this behavior is demonstrated in repeated annealing-exposure cycles. To explain these observations, we propose a mechanism based on changes in electrostatic and chemical boundary conditions through oxygen vacancy redistribution and the removal of surface adsorbates. © *2015 AIP Publishing LLC*. [http://dx.doi.org/10.1063/1.4918762]

Emergent functionalities at domain and twin boundaries[1] in oxide materials present rich fundamental physics, and hold significant promise for technological innovation. In particular, electrical conductance at ferroelectric domain walls in otherwise insulating wide-bandgap (multi)ferroics such as $BiFeO_3$ (Ref. 2) or $Pb(Zr_{0.2}Ti_{0.8})O_3$ (PZT)[3] has attracted much interest as a pathway towards domain-wall-based nanoelectronics.[4–6] The intrinsic conductance of charged domain walls[7,8] is related to the head-to-head or tail-to-tail orientation of the polarization vector, and therefore modifiable only by changes to the domain geometry itself,[9] limiting its applicability in device design. The segregation of defects such as oxygen vacancies preferentially at domain walls[10] — providing states within the band gap of the ferroelectric material for localised *extrinsic* conduction — offers a more promising pathway. Indeed, in $BiFeO_3$ thin films, persistent current footprints were recently observed at the initial position of domain walls, even after their displacement, pointing to a primarily extrinsic conductance.[11] Varying the growth conditions of such films to induce different oxygen vacancy densities was found to modulate the domain wall conductance by over an order of magnitude.[12,13] The defect states can also be photo-activated, temporarily inducing, or enhancing domain wall currents by supra-bandgap illumination.[14,15]

Here, we show that by using a moderate temperature, ultrahigh vacuum (UHV) annealing and ambient exposure, domain wall currents in PZT thin films can be reversibly controlled, allowing either conductive or insulating behavior, stable over the multi-week period of measurement. We propose a qualitative mechanism based on changes induced in surface adsorbates and oxygen vacancy distribution.

Combining dual frequency resonance tracking (DFRT) piezoresponse force microscopy[16] (PFM) and conductive-tip atomic force microscopy (CAFM) measurements[17] we probed PZT thin films epitaxially grown on $DyScO_3$ (110) (PZT_{DSO}) and $SrTiO_3$ (001) (PZT_{STO}) single crystal substrates, as represented in Figs. 1(a) and 1(b). The PZT_{DSO} films, 28–165 nm thick, were grown on 25 nm $SrRuO_3$ electrodes on (110) $DyScO_3$ single crystal substrates by pulsed-laser deposition,[18,19] and showed a low surface roughness of 0.3 nm root-mean-squared in scanned probe microscopy

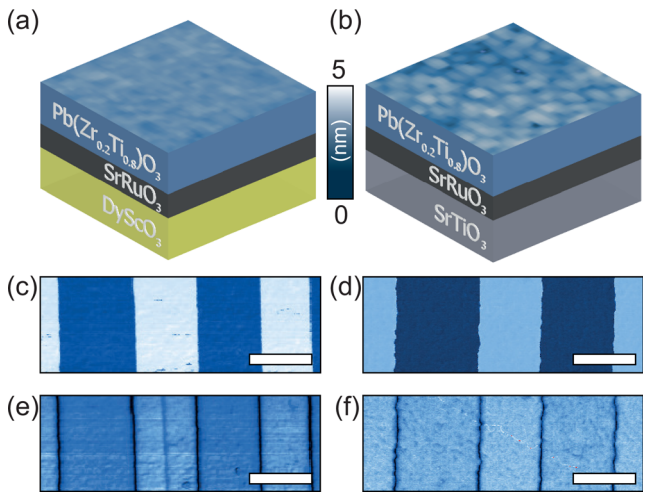

FIG. 1. SPM topography of a 1 μm^2 area in the schematically represented PZT_{DSO} ((a), 165 nm thick) and PZT_{STO} ((b), 70 nm thick) samples. PFM phase ((c) and (d)) and amplitude ((e) and (f)) images of stripe domains in the same films, with comparable 0.3 nm root mean square surface roughness. Compared to Czochralski-grown DSO substrates, Verneuil-grown STO substrates induce a higher density of oxygen vacancies and dislocations in the overlying PZT films, giving rise to visibly rougher domain walls. The white bar represents 1 μm.

a)Electronic mail: iaroslav.gaponenko@unige.ch

(SPM) topographical measurements, with sparse *a* domains (approximately one per $10\,\mu m^2$). The PZT_{STO} films, 60–70 nm thick, were grown on 30–40 nm metallic $SrRuO_3$ on (001) single-crystal $SrTiO_3$ substrates by off-axis radio-frequency magnetron sputtering, and showed similarly smooth surfaces without detectable presence of *a* domains. All samples are monodomain up-polarized (bright contrast in Figs. 1(c) and 1(d)) as-grown, so stripe domains were written with a positive-biased (+8 V) SPM tip scanned over the sample surface. We note that our previous studies on perovskite ferroelectrics[20,21] showed no significant differences in the structural or the functional properties between films grown on the same substrates by the two different methods, making the choice of substrate the defining parameter in our study. We could therefore compare domain wall transport in samples with very different oxygen vacancy densities and substrate chemical properties[22] but similar high crystalline[23,24] and surface quality.

In contrast to PZT_{STO}, where domain wall conduction is observed at low voltages, followed by displacement currents at higher voltages,[3] we detected no domain-wall-specific currents in as-grown PZT_{DSO}. Rather, both at domain walls and within the domain regions, we observe only insulating behavior at low voltages as shown by CAFM measurements with the tip bias incremented by −0.5 V every 10 lines in Fig. 2(b). From a tip bias of −4.5 V up to the maximum applied −9 V, irregular 10–100 pA currents are detected in the down-polarized written domain (Figs. 2(b) and 2(d)). The corresponding region is shown to have fully reversed in the subsequent PFM image (Fig. 2(c)). Meanwhile, in the as-grown up-polarized domains, we measure lower but more regular exponentially increasing leakage currents from −4.0 V onwards (Figs. 2(b) and 2(d)). Current acquired from the 100 nm region around the domain wall is simply an average of the signals from the neighbouring domains, as can be seen in Fig. 2(e). This *I-V* dependence can be related to nucleation-dominated polarization switching under negative tip bias in the down-polarized domains, giving rise to irregular displacement currents, and to charge injection and leakage with no polarization switching and more uniform currents in the up-polarized regions, as previously observed in $BiFeO_3$.[25]

Qualitatively similar behavior was observed in all four 28–165 nm PZT_{DSO} samples studied,[26] although the thinner films, in addition, present localized current hotspots throughout the sample, possibly related to pinholes. These results suggest that the domain wall conductance in PZT is not an intrinsic phenomenon, but strongly depends on the defect distribution in the sample, controlled by the growth conditions and substrate choice, and that a threshold density of defects, in particular of oxygen vacancies, is in fact necessary for current to be observed at the domain walls.

We then annealed the PZT_{DSO} samples for 30 min at ~300 °C in UHV. While under ambient conditions such moderate heating does not change either the crystalline quality or the macroscopic domain structure of PZT,[27] in UHV it should partially remove atmospheric adsorbates from the sample surface,[28] as well as favor the redistribution of oxygen vacancies.[29] Indeed, during the annealing, we observe a global reversal of the as-grown up-oriented polarization, consistent with significant changes in the electrostatic boundary conditions at the surface.[30] In some samples, the heat treatment led to surface deterioration and the formation of particulates, although in most cases high surface quality was maintained.

After the annealing, when identical PFM and CAFM measurements were repeated on new stripe structures (now written with negative −8 V tip bias since the polarization had reversed to down-oriented), distinct peaks in the average current signal can be seen at the position of the domain walls (Fig. 3(d)). Moreover, as shown in Figs. 3(b) and 3(e), the onset of these domain-wall-specific currents occurs at −2.0 V, before any detectable transport in the rest of the sample, and at low voltages not associated with polarization reversal. Within the domains, we observe qualitatively similar behavior to that in the untreated films. However, the onset of charge injection/leakage in the up-polarized regions is observed at a significantly lower threshold voltage of

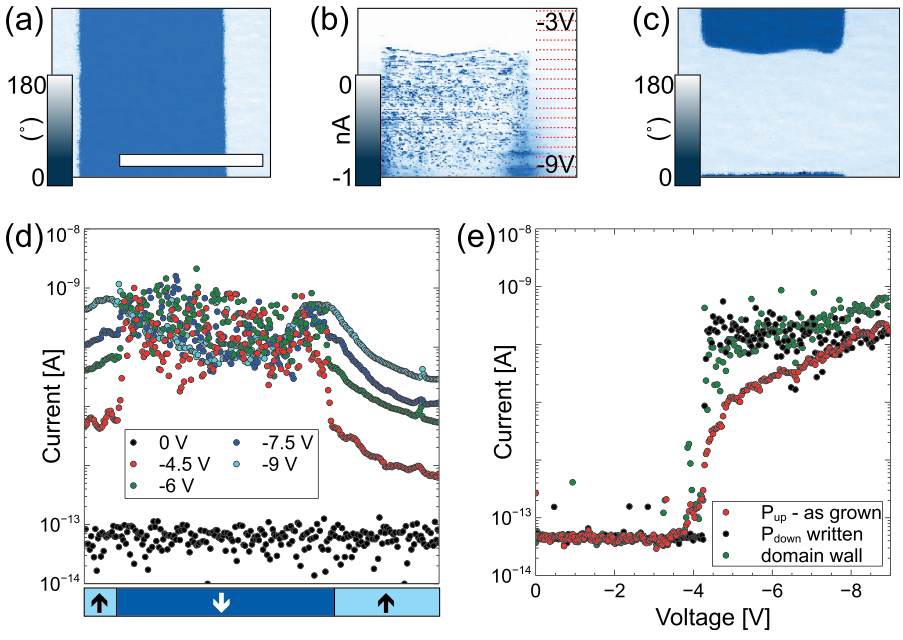

FIG. 2. Transport measurements in as-grown 165 nm PZT_{DSO}. (a) Initial PFM phase image of two domain walls. (b) CAFM measurement, with a −0.5 V increment of SPM tip bias at each interval indicated by the dashed red lines. (c) Subsequent PFM phase image of the same area, demonstrating that polarization switching accompanies the irregular currents observed throughout the down-polarized domain. (d) Average current levels as a function of position in (b) for varying tip bias, with color scale below indicating the polarization direction. (e) Current as a function of applied tip bias in the different regions, showing no domain-wall-specific conductance. The white bar represents 1 μm.

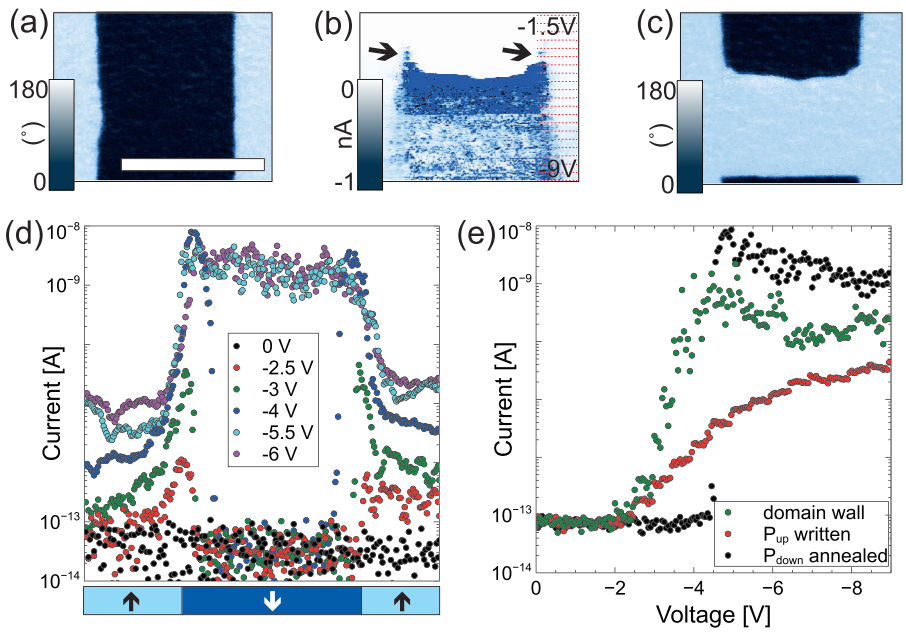

FIG. 3. Transport measurements in 165 nm PZT_{DSO} after thermal vacuum annealing. (a) Initial PFM phase image of two domain walls. (b) CAFM measurement with a −0.5 V increment in the SPM tip bias at each interval indicated by the dashed red lines. The change in contrast halfway down the image (tip bias −5 V) is related to a modification of the tip-sample contact. Arrows indicate domain wall segments, where no accompanying polarization reversal was observed in (c), subsequent PFM phase image of the same area. (d) Average current levels as a function of position in (b) for varying tip bias, with color scale below indicating the polarization direction. (e) Current as a function of applied tip bias, detected first specifically at the domain walls. The white bar represents 1 μm.

−2.5 V. In the down-polarized regions, abrupt onset of irregular switching currents still occurs at −4.5 V, but with higher current levels. The domain-wall-specific conductance could be measured throughout the two month duration of the experiment after the annealing process, as long as the sample was maintained under UHV.

To understand the microscopic mechanism governing the transport at 180° domain walls in PZT, we need to consider the differences between PZT_{STO} and PZT_{DSO}, as well as the role of thermal vacuum annealing. Since all samples are grown on $SrRuO_3$ thick enough to provide a good metallic bottom electrode, introduced into UHV from ambient, and show the same monodomain up-polarized state (promoting a higher density of oxygen vacancies near the film surface, and similar electrochemical interactions with atmospheric adsorbates), we can assume that the initial measurements take place under comparable electrostatic boundary conditions. During polarization switching the intense, highly localized electric field of the biased SPM tip which can reorganize/inject oxygen vacancies,[31] and allow them to preferentially segregate at the newly formed 180° domain walls[32] is likewise applied to all samples. The key difference is therefore the overall higher initial population of oxygen vacancies, determined by the choice of substrate.[22] As schematically shown in Fig. 4(b), this higher population of oxygen vacancies in as-grown PZT_{STO} allows the formation of a domain wall conducting channel through the film. In contrast, the oxygen vacancy population in PZT_{DSO} is apparently too low, preventing domain wall transport at sub-switching voltages, as illustrated in Fig. 4(a).

The effects of thermally annealing the PZT_{DSO} samples in UHV are more complex. The partial removal of surface adsorbates during such a process has been previously shown to affect screening[28] and lead to polarization reversal simply by varying the environmental conditions at moderate temperatures.[30,33,34] Moreover, even at low-to-moderate temperatures extremely oxygen-rich or oxygen-poor environments can lead to the formation of a surface "skin layer" with very different vacancy densities from the bulk.[29] Finally, oxygen vacancy mobility depends very strongly on temperature, with residence times varying from 10 000 s at 0 °C down to 0.0001 s at 150 °C.[35] We therefore posit that during the annealing process, the changes in the depolarizing field resulting from the partial removal of surface adsorbates and the accompanying polarization reversal are compensated by the rapid redistribution of oxygen vacancies, as schematically illustrated in Fig. 4(c). When a biased SPM tip is used to write domains in the annealed PZT_{DSO}, further injection/reorganization of oxygen vacancies at the 180° domain walls now allows a local conducting channel through the film. Clearly, this picture is only qualitative, and detailed measurements of oxygen vacancy densities at the domain walls and through the sample would be necessary to clarify it. It does, however, yield a testable prediction.

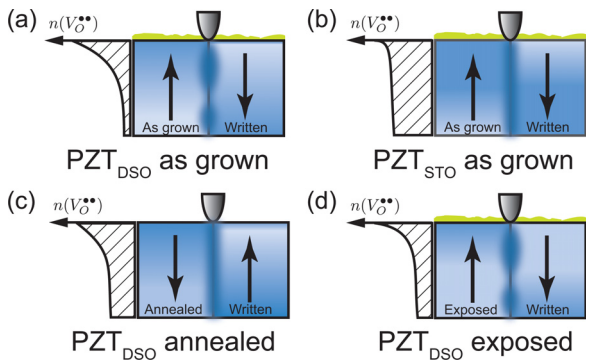

FIG. 4. Schematic illustration of the proposed qualitative model for adsorbate and oxygen vacancy dynamics effects on ferroelectric domain wall conductance. The as-grown state for both (a) PZT_{DSO} and (b) PZT_{STO}, screened by surface adsorbates and an increased density of oxygen vacancies (represented in shades of blue) near the sample surface. The higher overall population of oxygen vacancies in PZT_{STO} allows local conduction when these defects segregate at domain walls created with a biased SPM tip. (c) UHV annealing of PZT_{DSO} partially removes surface adsorbates, leading to polarization reversal and oxygen vacancy redistribution, and thus allows domain wall conductance. (d) Upon re-exposure to ambient conditions, surface adsorbate screening is re-established, again reversing polarization, and inhibiting conductance. Oxygen vacancy distribution at the domain wall is qualitatively represented on the left of the panel in each case.

Our qualitative picture implies that re-establishing full screening by surface adsorbates should reverse the observed effects on domain wall conductance, as schematically illustrated in Fig. 4(d). We tested this prediction by cycling the PZT_{DSO} samples between thermal annealing and atmospheric exposure. Upon re-exposure, the polarization of the films indeed reverts to the monodomain up-oriented state of the as-grown films, and no domain-wall-specific transport is observed for sub-switching voltages[26]. Subsequent re-annealing at ultrahigh vacuum again reverses the polarization to down-oriented, and allows domain-wall-specific current to be observed. We note, however, that repeated annealing/exposure cycling eventually results in local freezing-in of the down-polarized state and only partial reversibility of the transport characteristics, primarily due to increasing and permanent deterioration of the sample as the more volatile elements such as Pb are lost, as evidenced by the Energy-dispersive X-ray spectroscopy (EDX) measurements.[26] This effect could be mitigated by less aggressive and possibly more localized annealing. In addition, the reduced mobility of oxygen vacancies at room temperature compared to 300 °C could result in their incomplete screening of the depolarizing field, and thus the formation of compensating opposite polarity domains. We note that similar polarization switching had previously been reported in $BaTiO_3$ thin films analyzed in ultrahigh vacuum directly after growth with no air exposure, then confronted with controlled partial pressures of H_2O, leading to irreversible surface hydroxylation.[30] In our case, since the as-grown films are exposed to ambient conditions directly after deposition, all subsequent measurements probe the effects of adsorbate chemistry and oxygen vacancy dynamics beyond such an initial irreversible surface modification, and these, fortunately, appear to be largely reversible.

In conclusion, we show a reversible transition between insulating and conducting behavior at ferroelectric domain walls in PZT, induced by thermal annealing in UHV and subsequent re-exposure to ambient atmospheric conditions. Although we have demonstrated this reversible control of domain wall conductance only at the bulk level of the whole sample, our qualitative model suggests a possible pathway towards more targeted modulation. Using a SPM tip as a heat source[36] could provide nanoscale control over the thermal annealing process, and allow an extremely local tuning of the conductance characteristics of the domain walls in the parent material. Carbon-nanotube based CAFM probes are a particularly appealing candidate for such applications, as they demonstrate ultrahigh current carrying capabilities and high stability.[37]

The authors thank A. Klein, M. Alexe, and I. Stolichnov for helpful discussions, M. Lopes and S. Muller for technical support, and the Swiss National Science Foundation for financial support under Div II Grant No. 200021-153174.

[1]E. K. H. Salje, ChemPhysChem **11**, 940 (2010).
[2]J. Seidel, L. W. Martin, Q. He, Q. Zhan, Y.-H. Chu, A. Rother, M. E. Hawkridge, P. Maksymovych, P. Yu, M. Gajek, N. Balke, S. V. Kalinin, S. Gemming, F. Want, G. Catalan, J. F. Scott, N. A. Spaldin, J. Orenstein, and R. Ramesh, Nat. Mater. **8**, 229 (2009).
[3]J. Guyonnet, I. Gaponenko, S. Gariglio, and P. Paruch, Adv. Mater. **23**, 5377 (2011).
[4]H. Béa and P. Paruch, Nat. Mater. **8**, 168 (2009).
[5]G. Catalan, J. Seidel, R. Ramesh, and J. F. Scott, Rev. Mod. Phys. **84**, 119 (2012).
[6]R. K. Vasudevan, W. Wu, J. R. Guest, A. P. Baddorf, A. N. Morozovska, E. A. Eliseev, N. Balke, V. Nagarajan, P. Maksymovych, and S. V. Kalinin, Adv. Funct. Mater. **23**, 2592–2616 (2013).
[7]D. Meier, A. Cano, K. Delaney, Y. Kumagai, M. Mostovoy, N. A. Spaldin, R. Ramesh, and M. Fiebig, Nat. Mater. **11**, 284 (2012).
[8]T. Sluka, A. K. Tagantsev, P. Bednyakov, and N. Setter, Nat. Commun. **4**, 1808 (2013).
[9]P. Maksymovych, A. N. Morozovska, P. Yu, E. A. Eliseev, Y.-H. Chu, R. Ramesh, A. P. Baddorf, and S. V. Kalinin, Nano Lett. **12**, 209 (2012).
[10]J. H. Lee, R. H. Shin, and W. Jo, Phys. Rev. B **84**, 094112 (2011).
[11]I. Stolichnov, M. Iwanowska, E. Colla, B. Ziegler, I. Gaponenko, P. Paruch, M. Huijben, G. Rijnders, and N. Setter, Appl. Phys. Lett. **104**, 132902 (2014).
[12]J. Seidel, P. M. Y. Batra, A. Katan, S.-Y. Yang, Q. He, A. P. Baddorf, S. V. Kalinin, C.-H. Yang, J.-C. Yang, Y.-H. Chu, E. K. H. Salje, H. Wromeester, M. Salmeron, and R. Ramesh, Phys. Rev. Lett. **105**, 197603 (2010).
[13]S. Farokhipoor and B. Noheda, J. Appl. Phys. **112**, 052003 (2012).
[14]M. Schröder, A. Haussmann, A. Thiessen, E. Soergel, T. Woke, and L. M. Eng, Adv. Funct. Mater. **22**, 3936 (2012).
[15]S. Y. Yang, J. Seidel, S. J. Byrnes, P. Shafer, C.-H. Yang, M. D. Rossell, P. Yu, Y.-H. Chu, J. F. Scott, J. W. Ager III, L. W. Martin, and R. Ramesh, Nat. Nanotechnol. **5**, 143 (2010).
[16]B. J. Rodriguez, C. Callahan, S. V. Kalinin, and R. Proksch, Nanotechnology **18**, 475504 (2007).
[17]PFM and CAFM measurements were carried out in an Omicron VT AFM under UHV ($\sim 2 \times 10^{-10}$ mbar) using a Nanonis RC4 controller, with different commercial metallized tips. Typical scan size and rates were $2\times4\,\mu$m and 1.2 μm/s. For PFM, a 1 V, 300–400 kHz, AC tip bias was applied, and PFM signal measured with a dual Nanonis OC4 setup, following the DFRT method. For CAFM, a 0 to −10 V DC tip bias was applied, and current measured using a FEMTO DLPCA-200 preamplifier with a ±1 pA noise level. Initial measurements were carried out on samples introduced from ambient with no subsequent treatment. Vacuum annealing was carried out *in-situ* at ±350 °C for ∼30 min.
[18]J. Karthik, A. R. Damodaran, and L. W. Martin, Phys. Rev. Lett. **108**, 167601 (2012).
[19]J. Karthik, A. R. Domadaran, and L. W. Martin, Adv. Mater. **24**, 1610–1615 (2012).
[20]G. Catalan, H. Béa, S. Fusil, M. Bibes, P. Paruch, A. Barthélémy, and J. F. Scott, Phys. Rev. Lett. **100**, 027602 (2008).
[21]H. Béa, B. Ziegler, M. Bibes, A. Barthélémy, and P. Paruch, J. Phys.: Condens. Matter **23**, 142201 (2011).
[22]G. L. Yuan, L. W. Martin, R. Ramesh, and A. Uedono, Appl. Phys. Lett. **95**, 012904 (2009).
[23]J. Karthik and L. W. Martin, Phys. Rev. B **84**, 024102 (2011).
[24]S. Gariglio, N. Stucki, J.-M. Triscone, and G. Triscone, Appl. Phys. Lett. **90**, 202905 (2007).
[25]S. Farokhipoor and B. Noheda, Phys. Rev. Lett. **107**, 127601 (2011).
[26]See supplementary material at http://dx.doi.org/10.1063/1.4918762 for more details.
[27]P. Paruch and J.-M. Triscone, Appl. Phys. Lett. **88**, 162907 (2006).
[28]D. D. Fong, A. M. Kolpak, J. A. Eastman, S. K. Streiffer, P. H. Fuoss, G. B. Stephenson, C. Thompson, D. M. Kim, K. J. Choi, C. B. Eom, I. Grinberg, and A. M. Rappe, Phys. Rev. Lett. **96**, 127601 (2006).
[29]R.-V. Wang and P. C. McIntyre, J. Appl. Phys. **97**, 023508 (2005).
[30]J. Shin, V. B. Nascimento, G. Geneste, J. Rundgren, E. W. Plummer, B. Dkhil, S. V. Kalinin, and A. P. Baddorf, Nano Lett. **9**, 3720 (2009).
[31]S. V. Kalinin, S. Jesse, A. Tselev, A. P. Baddorf, and N. Balke, ACS Nano **5**, 5683 (2011).
[32]L. He and D. Vanderbilt, Phys. Rev. B **68**, 134103 (2003).
[33]R. V. Wang, D. D. Fong, F. Jiang, M. J. Highland, P. H. Fuoss, C. Thompson, A. M. Kolpak, J. A. Eastman, S. K. Streiffer, A. M. Rappe, and G. B. Stephenson, Phys. Rev. Lett. **102**, 047601 (2009).
[34]K. Garrity, A. Kakekhani, A. Kolpak, and S. Ismail-Beigi, Phys. Rev. B **88**, 045401 (2013).
[35]S. Gottschalk, H. Hahn, S. Flege, and A. G. Balogh, J. Appl. Phys. **104**, 114106 (2008).
[36]B. A. Nelson and W. P. King, in *Applied Scanning Probe Methods IV*, NanoScience and Technology, edited by B. Bhushan and H. Fuchs (Springer, Berlin, Heidelberg, 2006), pp 251–275.
[37]Y. Lisunova, I. Levkivskyi, and P. Paruch, Nano Lett. **13**, 4527–4531 (2013).